ADVANCED HEALTHCARE MATERIALS
www.advhealthmat.de

Multifunctional Liposomes for Image-Guided Intratumoral Chemo-Phototherapy

*Dyego Miranda, Kevin Carter, Dandan Luo, Shuai Shao, Jumin Geng, Changning Li, Upendra Chitgupi, Steven G. Turowski, Nasi Li, G. Ekin Atilla-Gokcumen, Joseph A. Spernyak, and Jonathan F. Lovell**

Intratumoral (IT) drug injections reduce systemic toxicity, but delivered volumes and distribution can be inconsistent. To improve IT delivery paradigms, porphyrin–phospholipid (PoP) liposomes are passively loaded with three hydrophilic cargos: sulforhodamine B, a fluorophore; gadolinium-gadopentetic acid, a magnetic resonance (MR) agent; and oxaliplatin, a colorectal cancer chemotherapeutic. Liposome composition is optimized so that cargo is retained in serum and storage, but is released in less than 1 min with exposure to near infrared light. Light-triggered release occurs with PoP-induced photooxidation of unsaturated lipids and all cargos release concurrently. In subcutaneous murine colorectal tumors, drainage of released cargo is delayed when laser treatment occurs 24 h after IT injection, at doses orders of magnitude lower than systemic ones. Delayed light-triggering results in substantial tumor shrinkage relative to controls a week following treatment, although regrowth occurs subsequently. MR imaging reveals that over this time frame, pools of liposomes within the tumor migrate to adjacent regions, possibly leading to altered spatial distribution during triggered drug release. Although further characterization of cargo loading and release is required, this proof-of-principle study suggests that multimodal theranostic IT delivery approaches hold potential to both guide injections and interpret outcomes, in particular when combined with chemo-phototherapy.

1. Introduction

Intratumoral (IT) injections of cytotoxic agents have potential to shrink or ablate tumors that are difficult to surgically resect. Obvious benefits include minimization of systemic toxicity compared to systemic administration, while achieving extremely elevated tumor drug biodistribution. IT injections have been developed as percutaneous local ablative therapies (PLATs), for treating hepatocellular carcinoma primary tumors.[1–3] PLATs typically involve IT injection of small molecules that are relatively safe at low concentration, such as ethanol[4–9] or acetic acid.[10–12] Photodynamic therapy (PDT), an ablative technique based on local generation of reactive oxygen species (ROS) by a light-exposed photosensitizer, has been proposed with IT injection of the photosensitizer.[13] IT injections of hafnium oxide nanoparticles as radiosensitizers have achieved improved tumor treatment.[14–16] Synergistic effects of magnetic hyperthermia and photothermal therapy caused by intratumoral iron oxide nanoparticles has been demonstrated to be effective in eradicating tumors.[17]

Despite the potential benefits, IT injections are not commonly used for most tumor treatments. This is due in large part to the variability of injections caused by intrinsic characteristics of solid tumors. Elevated interstitial fluid pressure (IFP) is a challenge for intratumoral injections.[18–23] This can cause partial efflux of the injected material through the needle track to the point of injection, thereby leading to uncertainty in the achieved dose.[24] High cell proliferation rates, abnormal lymphatics vascularization, and hydraulic conductivity caused by the permeability of tumor vessels contributes to increased IFP.[25–27] Increased extracellular matrix stiffness is also common in solid tumors. This rigidity not only increases IFP but can prevent the effective spread of the chemotherapeutical drugs within the tumor.[28–30]

IT-injected small hydrophilic molecules quickly drain out of tumors.[13,31] It has been shown previously that IT-injected liposomal cargo has delayed drainage compared to small molecules.[32,33] Porphyrin–phospholipid (PoP) liposomes are light-sensitive nanocarriers capable of controlled, on-demand, drug

D. Miranda, K. Carter, D. Luo, S. Shao, J. Geng, C. Li, U. Chitgupi, Prof. J. F. Lovell
Department of Biomedical Engineering
University at Buffalo
State University of New York
Buffalo, NY 14260, USA
E-mail: jflovell@buffalo.edu
S. G. Turowski
Department of Pharmacology and Therapeutics
Roswell Park Cancer Institute
Buffalo, NY 14263, USA
N. Li, Prof. G. E. Atilla-Gokcumen
Department of Chemistry
University at Buffalo
State University of New York
Buffalo, NY 14260, USA
Dr. J. A. Spernyak
Department of Department of Cell Stress Biology
Roswell Park Cancer Institute
Buffalo, NY 14263, USA
The ORCID identification number(s) for the author(s) of this article can be found under https://doi.org/10.1002/adhm.201700253.

DOI: 10.1002/adhm.201700253

release with near infrared (NIR) light exposure.[33–41] Thus, PoP liposomes are well-suited for chemo-phototherapy, an emerging modality that has numerous potential applications, and a variety nanocarriers have also been used for this purpose.[42–48] In this study, we develop a PoP liposome formulation that can stably load three different cargos for imaging and chemo-phototherapy. Multifunctional nanoparticulate approaches have been attracting interest recently for capabilities of both therapy and imaging.[49–54] Triggered delivery approaches promise to provide a better controlled release of drugs from nanoparticles[55–59] Multimodal imaging can be used to extract diverse information about nanoparticle behavior.[60] Here, multimodal imaging is used to monitor PoP liposome cargo behavior following IT-injection (at drug doses hundreds of times lower than conventional systemic doses) and provide insights into the observation that delaying the interval between injection and light treatment improved outcomes.

2. Results and Discussion

2.1. PoP Liposomes for Passive Cargo Loading and Light-Induced Release

Various lipids were assessed to develop a formulation for passive cargo entrapment and light-triggered drug release. Sulforhodamine B (SRB) was used as a hydrophilic fluorescent cargo loaded at 50×10^{-3} M (a self-quenching concentration) to report on cargo release. The liposomes in this study had a fixed molar ratio of 50% cholesterol (Chol), 5% 1,2-distearoyl-sn-glycero-3-phosphoethanolamine-*N*-(methoxy(PEG)-2000 (MPEG-2000-DSPE), and 2% sn-1-palmitoyl sn-2-pyropheophorbide phosphatidylcholine (pyro-lipid (PoP)). Different phospholipids, namely 1,2-dioleoyl-sn-glycero-3-phosphocholine (DOPC), 1,2-distearoyl-sn-glycero-3-phosphocholine (DSPC), 1,2-dipalmitoyl-sn-glycero-3-phosphocholine (DPPC), 1,2-dimyristoyl-sn-glycero-3-phosphocholine (DMPC), or sphingomyelin (SPM) were used as primary lipids in PoP liposomes. Light-triggered release tests using a 665 nm laser demonstrated a fast release rate when liposomes were formulated with the unsaturated lipid DOPC, but not with saturated ones, regardless of side chain length (**Figure 1**A). Conversely, cargo retention stability in 50% serum of liposomes formed from saturated lipids was superior to those made with DOPC (Figure 1B). Increasing amounts of saturated lipids, such as DSPC, have been shown to induce higher lipid packing and stability in other light-triggered liposome systems.[61] To obtain liposomes with both fast laser release and good serum stability, saturated and unsaturated lipids were blended at different molar ratios and assessed. Liposomes containing a molar ratio of [1:3] of [DOPC:DSPC] exhibited fast NIR light-induced release (Figure 1C) without compromising serum stability (Figure 1D). This ratio was thus chosen to be used throughout this study. The speed of light-triggered release was influenced by the amount of PoP in the bilayer, with increasing rates from 0.5% to 5% PoP, while liposomes lacking without PoP did not release cargo (Figure S1, Supporting Information). When normalizing the release rate by the amount of PoP presents in the liposomes a maximum efficiency achieved with 2% PoP, (Figure 1E). Our group recently reported that PoP liposomes containing unsaturated lipids exhibit accelerated light-triggered cargo release.[34] Unsaturated lipids were oxidized during the process, which likely induced bilayer destabilization, although permeabilization was found to be transient. Photooxidation methods have

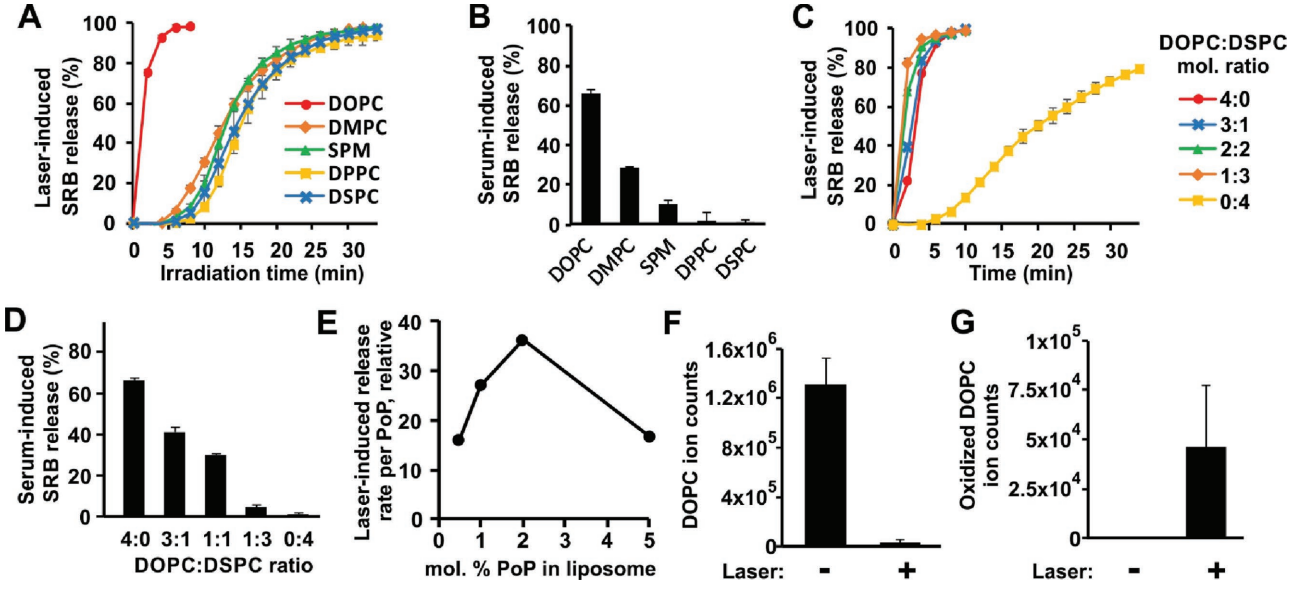

Figure 1. A PoP liposome formulation for NIR release of passively loaded cargo. A) Light-triggered release of SRB using a 300 mW cm^{-2} 665 nm laser with PoP liposomes containing the indicated lipids (43 mol%), together with 50 mol% Chol, 5 mol% PEG-lipid, and 2 mol% PoP. B) Serum stability of these formulations at 37 °C in 50% bovine serum. C) Light-triggered release of SRB from PoP liposomes containing indicated ratios of DOPC:DSPC. D) Serum stability of PoP liposomes with different ratios of DOPC:DSPC. E) Laser-induced SRB release rate (normalized by PoP content) of liposomes containing 1:3 ratio of DOPC:DSPC and the indicated mol% PoP. F) Ion counts for DOPC (m/z = 786.6007, $[M+H]^+$) in PoP liposomes with or without NIR laser irradiation. G) Ion counts for oxidized DOPC (m/z = 850.5804, $[M+H]^+$) in PoP liposomes with or without NIR laser irradiation.

been widely used to trigger cargo release from liposomes.[62] To test if a similar mechanism existed here, we investigated the levels of DOPC and potential oxidized products before and after laser irradiation, using liquid chromatography quadrupole time of flight mass spectrometry (LC-QTOF) as described previously.[34] As expected, after laser irradiation there was a profound decrease in DOPC (Figure 1F) and appearance of a new species (Figure 1G), which was determined as oxidized DOPC based on MS/MS characterization. Thus it is likely that DOPC accelerated cargo release via POP-mediated photooxidation and subsequent bilayer destabilization.

2.2. SRB, Gd-DTPA, and Oxaliplatin Coentrapment and Release

The developed PoP liposome formulation was next used to coencapsulate SRB, gadolinium-gadopentetic acid (Gd-DTPA), and oxaliplatin (OX). Liposomes were formed with a buffer of 50×10^{-3} M SRB (27.9 mg mL^{-1}), 200×10^{-3} M Gd-DTPA (109.5 mg mL^{-1}), and 12.59×10^{-3} M OX (5 mg mL^{-1}). This SRB concentration was sufficient for robust self-quenching inside liposomes, the OX concentration used is close to the solubility limit, and the Gd-DTPA concentration was selected based on how it influenced liposome size (Figure S2, Supporting Information). An increased concentration of Gd-DTPA resulted in larger liposome size, possibly due to effects related to high ionic strength or osmolarity of the solution. SRB fluorescence self-quenching was found to decrease with increasing Gd-DTPA concentration (Figure S3, Supporting Information), possibly by reducing SRB overall encapsulation efficiency within the aqueous liposome core. As liposomes containing 200×10^{-3} M Gd-DTPA resulted in a size smaller than 200 nm while retaining good SRB stability and fluorescence response after laser treatment, those were selected to be used as standard liposomes for our study. Inductively coupled plasma (ICP) analysis revealed that after encapsulation and removal of unentrapped cargo, the total concentration of Gd and Pt present in Gd-DTPA and OX, respectively, was 503 μg mL^{-1} (≈1.75 mg mL^{-1} or $\approx 3.2 \times 10^{-3}$ M Gd-DTPA) and 27 μg mL^{-1} (≈54.7 μg mL^{-1} or $\approx 138 \times 10^{-6}$ M OX), respectively. The drug loading percent (DL%) for both Gd-DTPA and OX was found to be 4.2% and 0.34%, respectively. This OX loading is substantially lower than previous reports of liposomal OX, demonstrating that further optimization of cargo entrapment is required.[63,64] Due to the hydrophilic nature of the cargos, they are expected to be located in the aqueous lumen of the liposomes. SRB:Gd-DTPA:OX PoP liposomes showed faster light-induced SRB release (≈40 s) (**Figure 2**A) compared to all the other PoP liposome formulations containing only SRB (Figure 1C). Detection of light-induced cargo release was assessed using microcentrifugal filtration separation. SRB release could be visualized by naked eye during these three time-points (Figure 2B). SRB and PoP fluorescence were determined for each time point in both filtrate and retentate fractions (Figure S4, Supporting Information), and fluorescence values of SRB were converted to concentration values based on a standard SRB fluorescence curve. Based on ICP analyses, Gd and Pt were concurrently released after 2 min laser treatment but at different final concentrations (SRB = 98 μg mL^{-1}; Gd = 329 μg mL^{-1}; Pt = 22.4 μg mL^{-1}) (Figure 2C). This is significant because since all three cargos are released at correlated rates, so that SRB can potentially serve as a proxy for drug release and Gd-DTPA can potentially serve as a proxy for drug distribution. Differences in

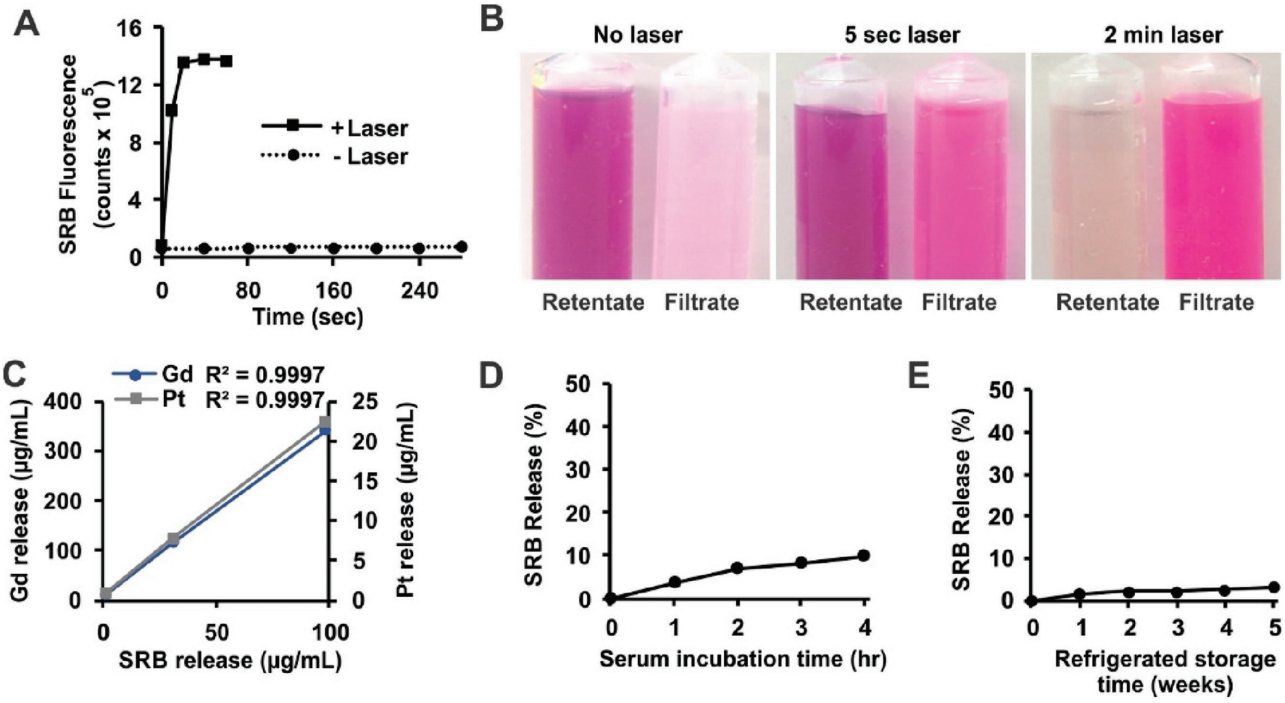

Figure 2. Multicargo release from PoP liposomes containing SRB:Gd-DTPA:OX. A) SRB release from liposomes coencapsulating SRB, Gd-DTPA, and OX with or without 665 nm laser irradiation. B) Centrifugal filtration of liposomes treated with laser. C) Gd and Pt release as a function of SRB release. D) Serum stability of SRB:Gd-DTPA:OX PoP liposomes at 37 °C in 50% bovine serum. E) Storage stability of SRB:Gd-DTPA:OX PoP liposomes at 4 °C.

release rates could be attributed to differences in cargo physicochemical properties or cargo–cargo interactions and further study is required. SRB:Gd-DTPA:OX PoP liposome diameter before and after 2 min laser treatment was 171 and 153 nm, respectively (Figure S5, Supporting Information). The polydispersity changed slightly from 0.28 to 0.23 with laser treatment. Transmission electron microscopy revealed spherically shaped liposomes of variable size (Figure S6, Supporting Information). The variable size can be attributed to the relatively high polydispersity as the particles were not extruded during liposome production.

When incubated at 37 °C in 50% mature bovine serum for 4 h, SRB release in SRB:Gd-DTPA:OX PoP liposomes was found to be ≈10% (Figure 2D). SRB:Gd-DTPA:OX PoP liposomes were assessed for refrigerated storage stability in phosphate buffered saline (PBS) (Figure 2E). After five weeks of storage, SRB release was found to be ≈3%. Therefore, this formulation presents excellent storage stability and good stability in serum.

2.3. Cell Viability

CT26.WT murine colon cancer cells were incubated with SRB:Gd-DTPA:OX PoP liposomes or free OX for 48 h (**Figure 3**). The final concentration was adjusted to 5 or 25×10^{-6} M OX. Both free and encapsulated OX caused cell toxicity, however encapsulated OX was less cytotoxic compared to the free drug at higher concentrations. Uptake of intact neutral liposomes by cells can occur via endocytosis, followed by additional intracellular trafficking.[65] Cytotoxicity further increased for PoP liposome samples when exposed to laser treatment. The mechanism is likely a combination of singlet oxygen generation and the released drug having better bioavailability. Some liposomes were pretreated with laser prior incubation to avoid ROS caused by PoP. Pretreated liposomes induced higher toxicity when compared to those that did not receive laser treatment, which is likely due to drug release and greater bioavailability. We attributed observed cytotoxicity effects to released OX, however the effects of SRB and Gd-DPTA could have partially contributed as well. Pretreated liposomes were less toxic to those treated in situ, which was likely due to the PDT effect during treatment. The highest cytotoxicity occurred with 25×10^{-6} M OX in PoP liposomes and irradiation, resulting in nearly complete cell kill.

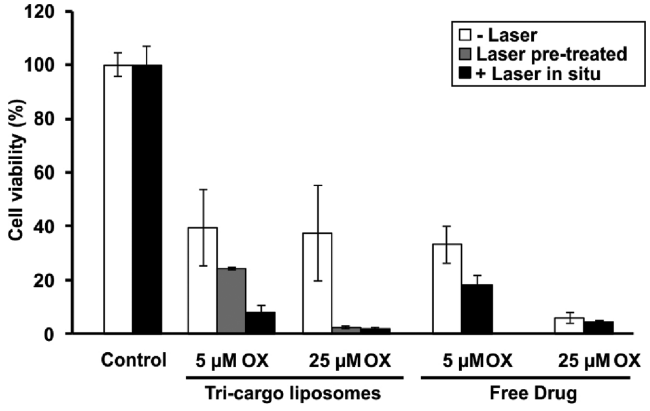

Figure 3. In vitro chemo-phototherapy. CT-26 cell viability following treatment with indicated liposomes or free drug with or without laser treatment. Viability was measured 48 h after incubation by XTT assay.

2.4. Intratumoral Liposome Latency

To test liposome behavior within tumors, 40 μL of SRB:Gd-DTPA:OX PoP liposomes were injected at four locations per tumor (10 μL per injection), in mice with dual contralateral tumors (**Figure 4**A). One side was irradiated 10 min after injection, while the contralateral tumor was covered to minimize stray light exposure. Even though SRB:Gd-DTPA:OX PoP liposomes were shown to fully release its cargo in less than 2 min in vitro, due to concerns about light attenuation in tissues, we opted to increase the light irradiation time to 30 min. With irradiation, SRB release and unquenching were observed in the tumor. Based on longitudinal imaging of SRB, liposomes that received laser treatment right after injection quickly released SRB throughout the tumor area but after 2 h there was noticeable decrease in fluorescence, consistent with expected rapid drainage of small hydrophilic molecules from tumors. Most released SRB quickly cleared from the tumor (Figure 4B), while SRB fluorescence could be detected in the abdominal region in the following hours, presumably due to systemic clearance. After 24 h, the contralateral tumor was then irradiated and again SRB fluorescence increased dramatically. This shows not only that liposomes were persistent in the tumor over 24 h but they also maintained their cargo without leakage, since SRB was maintained at self-quenching concentrations. The mice were imaged again 2 h after laser treatment and interestingly, SRB fluorescence was more persistent than in tumors irradiated immediately after injection. The high fluorescence persisted even at 6 h after irradiation. When the SRB values were normalized (Figure 4C), tumors irradiated 24 h after injection had a slower SRB drainage rate compared to tumors irradiated immediately after injection. The reason for the slower drainage rate with a longer drug-light-interval is unclear, but it might be related to more homogenous liposome distribution throughout the tumor. We hypothesized OX would have increased efficacy if we give a 24 h drug-light-interval based on slower drainage rate.

2.5. Survival Studies

To investigate efficacy of SRB:Gd-DTPA:OX PoP liposomes in vivo, liposomes were injected IT at four locations (40 μL in total, 10 μL per injection) in mice bearing single CT-26 tumors. Mice were divided into five groups: (1) + Laser: Mice irradiated 10 min after injection; (2) 24 h + Laser: Mice treated with laser 24 h after injection; (3) Empty + Laser: Mice injected with empty PoP liposomes with laser treatment immediately after injection; (4) – Laser: Mice injected with SRB:Gd-DTPA:OX PoP liposomes but did not receive any laser treatment; (5) Control: Mice that did not receive any injection or laser treatment. Tumor size was measured every 2–3 d until they reach tenfold their original size, then mice were sacrificed. During the first 7 d (16 d in Figure S7, Supporting Information), mice

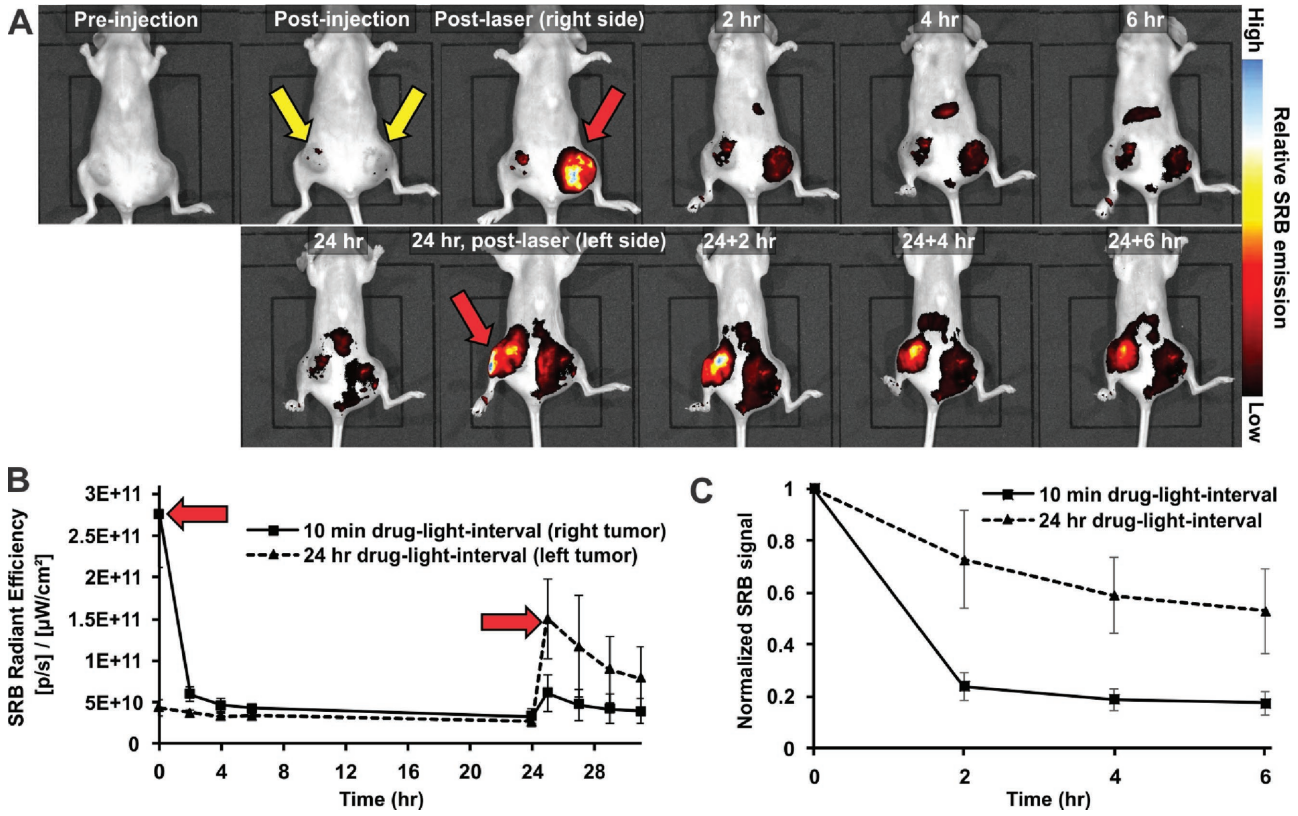

Figure 4. SRB drainage and release with photoactivatable liposomes. A) BALB/c mice with dual CT-26 tumors were IT-injected with SRB:Gd-DTPA:OX PoP liposomes (yellow arrows). Initially, only one side was treated with a 665 nm laser (red arrow). The contralateral tumor was treated 24 h later. Signal shows SRB fluorescence, which is self-quenched in intact liposomes. B) SRB signal and persistence in the dual tumor model. Red arrows show point of tumor irradiation. C) Normalized SRB drainage immediately following laser irradiation in dual tumor model. Values show mean +/− std. dev. for $n = 6$ mice.

from group 2 showed significant delay in tumor growth percent when compared to groups 3, 4, and 5 ($p = 0.0002$; 0.00007; 0.00008, respectively, Student's *t*-test), approaching statistical significance when compared to group 1 ($p = 0.089$. Student's *t*-test) (**Figure 5**A). No groups were completely cured and fast tumor growth occurred in group 2 in the second week.

For survival analysis (Figure 5B), mice from group 2 (24 h + laser) had a significant increase in survival time when compared to controls ($p = 0.0025$, Log-rank test) but not significant when compared to group 1 ($p = 0.176$, Log-rank test). Controls and groups 3 and 4 had to be sacrificed sooner than those from the chemo-phototherapy groups 1 and 2. For these groups, there was an initial shrinkage in the region where the liposomes were injected, by observing the tumor mass reduction or temporary absence of tumor growth in that region after the treatment when compared to noninjected sites. This

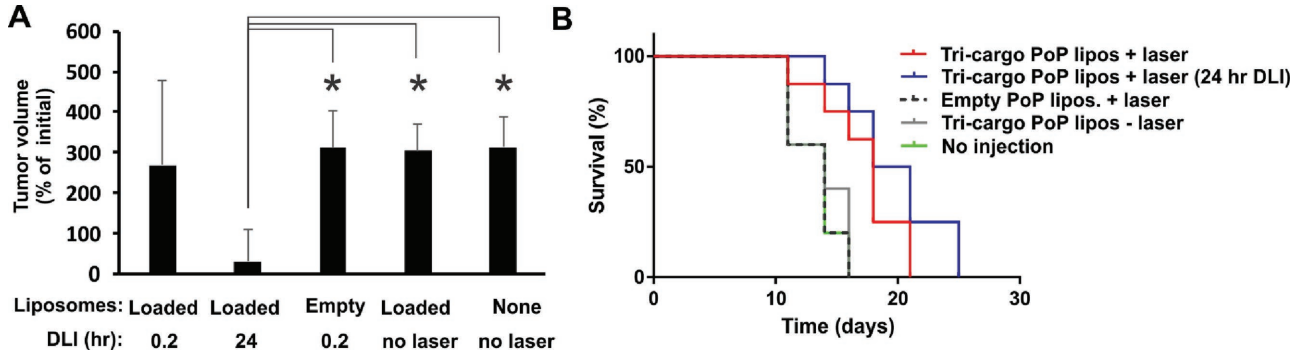

Figure 5. IT chemo-phototherapy antitumor efficacy. A) Tumor growth one week after treatment with tricargo liposomes (0.08 mg kg^{-1} OX or equivalent; 30 min. laser irradiation at 665 nm, fluence rate: 300 mW cm^{-2} with indicated drug-light-interval (DLI)). Based on pairwise two-tailed student *t*-test, the 24 h DLI group had significantly smaller tumors than groups indicated with asterisks ($p < 0.0005$). B) Survival of treated mice. Mice were sacrificed when tumor volume reached 10 times initial. $n = 8$ for the two groups receiving drug and laser and $n = 5$ for the other groups.

was evident especially in group 2, where not only tumors had a significant tumor shrinkage, but mice had the best survival. Liposomes act as an extra protection layer to the drug, slowing the drainage of small molecules, which upon 24 h delay prior to laser treatment, can enhance the drug distribution to other tumor sites. Similar behavior has been observed using macrophages as carriers of nanoshells for photothermal therapy.[66] Although all mice tolerated the treatment, toxicity studies were not performed in this preliminary proof of principle work. However, we note that the injected doses of OX were hundreds of times less than conventional systemic preclinical OX doses in in the literature. Liposomal OX can be dosed with multiple intravenous doses of 5 mg kg^{-1} (compared to 0.08 mg kg^{-1} in this study).[67] The PoP used in this work was previously demonstrated not to induce acute systemic toxicity at extremely high intravenous doses of 1 g kg^{-1}.[68]

2.6. MR Imaging

Magnetic resonance imaging (MRI) is a noninvasive imaging technique used in both clinical and research settings. Contrast agents provide a tool to visualize IT injections, helping to localize, in real time, needle positioning and sample deposition at specific tumor sites. Gd-DTPA is a clinical contrast agent and the viability of SRB:Gd-DTPA:OX PoP liposomes for MR was initially tested in vitro. At temperatures of 25 and 37 °C, both the laser and detergent treated liposomes showed significantly higher T1 relaxivities over the untreated liposomes (**Table 1** and Figure S8 (Supporting Information)). The higher relaxivities of the treated liposomes is indicative of increased water interaction with the contrast agent no longer enclosed within the liposome. Interestingly, increasing the temperature from 25 to 37 °C had the opposite effect on the relaxivities of control and treated liposomes. The reduction in relaxivities in the treated liposomes at higher temperatures (≈15% decrease, on average) is a documented phenomenon[69,70] and is attributed to increased molecular tumbling rates that result in less efficient relaxation.[71] However, control liposomes demonstrated a 28% increase in both T1 and T2 relaxivities at the higher temperature. This may be due to increased diffusion of water across the liposomal membrane enabling more efficient proton relaxation although further exploration of this phenomenon is needed. A similar increase in T1 relaxivity upon temperature increase was documented in thermosensitive liposomes for six clinically approved nonionic Gd-based MRI contrast agents prior to the liposome reaching its melting point.[72]

Table 1. Influence of temperature on T1 and T2 relaxivities. Liposomes irradiated with laser or exposed to detergent (Triton X-100) presented higher T1 relaxivities compared to untreated intact liposomes.

Formulation	25 °C		37 °C	
	$r1$ [mM s]$^{-1}$	$r2$ [mM s]$^{-1}$	$r1$ [mM s]$^{-1}$	$r2$ [mM s]$^{-1}$
Intact tricargo liposomes	1.16	1.82	1.49	2.33
+ Laser	2.00	2.36	1.63	2.16
+ Detergent	1.99	2.64	1.75	2.02

To understand the IT behavior of the liposomes, MR images were acquired in mice prior to, immediately after and up to 72 h after IT injection. A volume of 20 µL was injected from both the superior and inferior sides of the tumor. Laser treatment was not applied in this study so that the kinetics of distribution of the liposomes could be observed. 3D distribution of the liposomes was readily detectable by MR imaging as hyperintense regions (**Figure 6**). MR imaging revealed multiple

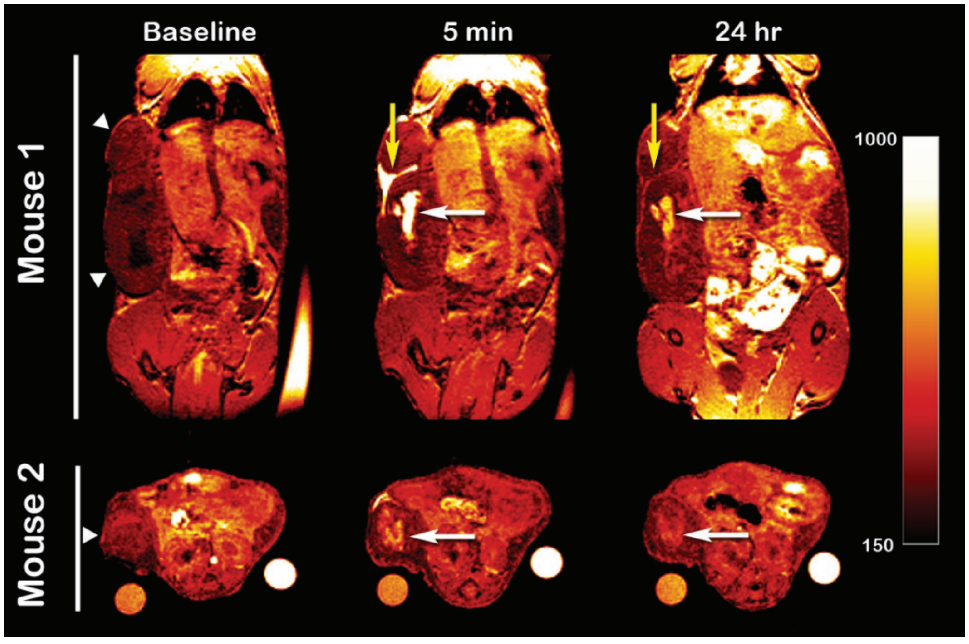

Figure 6. MR imaging. MR images of two mice (top, coronal view; bottom, axial view) IT-injected with SRB:Gd-DTPA:OX PoP liposomes (injection sites are shown with white arrowheads). After injection, IT MR enhancement was observed (white arrows). Temporary subcutaneous MR enhancement was observed following injection (yellow arrow, top row), indicative of either poor needle placement or liposome efflux.

distribution behaviors within the tumor over the course of 24 h (Figure S9, Supporting Information). Areas of accumulation near tumor border or subcutaneous regions cleared rapidly, presumably due to increased access to vasculature and lymphatics. The bright areas in stomach and intestines were caused by food following feeding. Additionally, some areas with highly localized deposition experienced an outward diffusion of the liposomes to a greater localized volume. Finally, some areas within the tumor that did not show enhancement immediately after injection showed enhancement 24 h later, indicating a migration of liposomes from another location of the tumor. This indicates local influences such as interstitial pressure, stromal content, and necrotic channels may result in a heterogeneous distribution of liposomes following injection that can be detected with 3D MR imaging.

3. Conclusion

A PoP liposome formulation was developed with a molar ratio of 1:3 unsaturated to saturated phospholipids to entrap hydrophilic cargos with good serum stability and fast light-triggered release. PoP liposomes passively entrapped and concurrently released three different cargos: SRB, Gd-DTPA, and OX. With IT injection, the drug-light-interval affected drainage of light-released cargo based on fluorescence imaging and also impacted antitumor efficacy. Chemo-phototherapy was found to be significantly more effective than IT injection of drugs alone or IT PDT alone, one week post-treatment. MRI of encapsulated Gd-DTPA revealed the pooling and spread of liposomes over time that might account for the observed superiority of a longer drug-light interval. Together, these results underscore how multimodal imaging and therapy results can aid IT-based therapies, particularly in the context of chemo-phototherapy.

4. Experimental Section

Materials: Lipids purchased from Corden Pharma include DOPC (#LP-R4-070), DSPC (#LP-R4-076), DPPC (#LP-R4-057), DMPC (#LP-R4-058), cholesterol (#CH-0355), 1,2-distearoyl-sn-glycero-3-phosphoethanolamine-*N*-(methoxy(PEG)-2000 (MPEG-2000-DSPE, #LP-R4-039). SPM was purchased from NOF America (#Coatsome NM-10). sn-1-palmitoyl sn-2-pyropheophorbide phosphatidylcholine (pyro-lipid (PoP)) was synthesized as previously described.[68] Diethylenetriaminepentaacetic acid gadolinium(III) dihydrogen salt hydrate (Gd-DTPA) was purchased from Sigma-Aldrich (#381667). SRB was purchased from Biotium (#80100). OX was obtained from LC laboratories (#O-7111). Sterile mature bovine serum was purchased from Pel-Freez (#37218-5). Other reagents used in experiments were purchased from Sigma and prepared in our laboratory using Type 1 reagent grade water (Nanopure, Barstead).

Preparation and Characterization of PoP Liposomes: Unless stated otherwise, for most experiments, liposomes were constituted of DOPC:DSPC:Chol:DSPE-PEG:PoP at a molar ratio of 10.75:32.25:50:5:2 mol%. For a few experiments different formulations and phospholipids (DMPC, DPPC, and sphingomyelin) were used. Liposomes were prepared by the thin-film hydration method. Briefly, lipids (40 mg) dissolved in 1 mL chloroform and mixed in borosilicate test tubes. The organic solvent was then evaporated under gentle nitrogen flow until a lipid film was formed at the bottom of the tube. Samples were incubated in a vacuum chamber for 4 h in order to further remove chloroform from the lipid film. For the hydration step, 1 mL of a 50×10^{-3} M SRB solution (with or without 5 mg mL^{-1} OX and 200×10^{-3} M Gd-DTPA) was heated to 60 °C and added to the lipid film. Samples were sonicated in a water bath for 30 min at 60 °C. In order to remove the unencapsulated components, size-exclusion chromatography was used. Columns containing Sephadex G-75 were loaded with 1 mL of liposomes. Fractions with high concentration of liposomes were collected and combined. The sample was then dialyzed twice against PBS (137×10^{-3} M NaCl, 7×10^{-3} M Na_2HPO_4, 3×10^{-3} M NaH_2PO_4, pH 7.4) and stored protected from light at 4 °C. Based on dynamic light scattering, SRB:Gd-DTPA:OX PoP liposomes had a zeta potential of −26 mV and a size of 171 nm. Drug Loading percent (DL%) was calculated using a previously reported formula for lipid nanoparticles.[73]

Light-triggered cargo release from PoP liposomes was performed with a power-tunable 665 nm laser diode (RPMC laser, LDX-3115-665). The fluence rate was set to 300 mW cm^{-2} and in vitro release was performed in both 50% sterile bovine serum and/or PBS at 37 °C. SRB fluorescence was constantly monitored using a fluorimeter (PTI) at 585 nm emission wavelength.

For serum stability tests, liposomes were added to 50% sterile mature bovine serum and incubated at 37 °C during 3–4 h with SRB fluorescence (+/− Triton X-100) being measured hourly using a TECAN Safire fluorescence microplate reader. The size and polydispersity of PoP liposomes were determined by dynamic light scattering in a NanoBrook 90 plus PALS.

The concentration of Gd and Pt metals present in both Gd-DTPA and oxaliplatin encapsulated in SRB:Gd-DTPA:OX PoP liposomes was determined by inductively coupled plasma atomic emission spectroscopy (ICP-OES). Briefly, 100 µL of the stock liposomes solutions were digested in 100 µL of concentrated metal grade HNO_3 at 60 °C for 1 h. After digestion, the volume was adjusted to 10 mL with water. Blank solutions were prepared by adding 100 µL of concentrated metal grade HNO_3 in 9.9 mL purified water. In order to obtain the concentration of Gd and Pt released from liposomes before, during and after laser treatment, samples were prepared by adding 200 µL of stock liposomes solution to 800 µL of PBS and treated or not with 665 nm laser. The samples were centrifuged at 4000 g using 100 kDa molecular weight cut-off 5 mL Microsep tubes (Pall Corporation, #MPC100C41) until the filtrate volume reached about 1 mL, then, 1 mL water was added to the retentate, resuspended and the samples were centrifuged again until the filtrate had a final volume of ≈2 mL. The final volume of both filtrate and retentate were adjusted to 2 mL with water. Each 2 mL sample was digested with 100 µL of concentrated metal grade HNO_3 at 60 °C for 1 h. After digestion, the samples had their volume adjusted to 10 mL with water before ICP-OES analysis.

LC-QTOF Characterization of DOPC and Potential Oxidation Products: Liposomes were diluted in PBS after irradiation. The lipid content of 1 mL of treated and untreated liposomes was then extracted using a modified Bligh–Dyer method[74] and lipid extracts were prepared as we described previously.[34] Lipids were resuspended in chloroform for LC-MS analysis. Data acquisition was performed using LC-ESI-QTOF (Agilent 1260 HPLC coupled to Agilent 6530 Accurate-Mass Quadrupole Time-of-Flight instrument, Agilent Technologies, Santa Clara, CA, USA) in positive electrospray ionization mode. Data were collected using an m/z range 50–1700 in extended dynamic range. For targeted analysis of DOPC and oxidized DOPC, the corresponding m/z for each ion (for DOPC m/z = 786.6007, [M+H]+; and for oxidized DOPC m/z = 850.5804 [M+H]+) was extracted in MassHunter Qualitative Analysis (version B.06.00, Agilent Technologies). Peak areas for each ion in extracted ion chromatograms (EICs) were manually integrated and were presented as ion counts. The identity of m/z = 786.6007 and 850.5804 were confirmed by MS/MS at 15, 35, and 55 V (details can be found in the work of Luo et al.[34]). Based on m/z = 184.0728, 522.3533, 86.0985 fragments, m/z = 786.6007 is confirmed as DOPC; and, similarly, based on m/z = 832.5724, 814.5698, 184.0844 fragments, m/z = 850.5804 was confirmed as oxidized DOPC.

Cell Viability: CT26.WT colon cancer cells were maintained at 37 °C, 5% CO_2 in Dulbecco's Modified Eagle's Medium containing 10%

fetal bovine serum and 1% penicillin/streptomycin. 1×10^4 cells were cultured on a 96-well plate. SRB:Gd-DTPA:OX PoP liposomes or free drug samples (54.7 μg mL^{-1}) were added to cells containing complete media and incubated for 48 h. Media was removed post-treatment and the cells were washed with PBS before adding fresh media containing serum. Cells were immediately exposed to laser by placing the 96-well plate in a 665 nm light-emitting diode box. Cells were irradiated for 20 min at a fluence of 35.8 J cm^{-2} (fluence rate: 29.84 mW cm^{-2}). Viability was assessed with the 2,3-bis(2-methoxy-4-nitro-5-sulfophenyl)-2H-tetrazolium-5-carboxanilide (XTT) assay. 24 h after laser treatment, media was replaced with XTT solution after the cells were washed with PBS. XTT solution was prepared by adding 50 μg mL^{-1} of XTT and 30 μg mL^{-1} *N*-methyl dibenzopyrazine methyl sulfate to PBS. 100 μL of XTT stock solution was added to each well and incubated 2 h before reading the absorbance at 450 and 630 nm (background). Cell viability was calculated as ratio of absorbance of treated cells to untreated cells. All measurements were performed in triplicate and error bars indicate standard deviation.

SRB Drainage, Tumor Growth, and Survival Experiments: Mouse experiments were performed in accordance to protocols that approved by the Institutional Animal Care and Use Committees of University at Buffalo and Roswell Park Cancer Institute. Seven to eight week old female BALB/c mice (Envigo) were injected with 1×10^6 CT26.WT colon carcinoma cells (ATTC, #CRL-2638) in the right flank (32 mice) and in both right and left flank for SRB drainage experiments (6 mice). When tumors reached a size of 5–7 mm, mice received intratumoral injections (40 μL) of SRB:Gd-DTPA:OX PoP liposomes at four different sites (at a dose of 32 mg kg^{-1} lipids, which contained ≈2.8 mg kg^{-1} Gd-DTPA and 0.08 mg kg^{-1} OX). Irradiation of intratumoral PoP liposomes was performed by using a power-tunable 665 nm laser diode (RPMC laser, LDX-3115-665) for 30 min. Fluence rate was set to 300 mW cm^{-2}, with a spot size of 10 mm in diameter. All mice were anesthetized with 4% isoflurane and maintained at 2% during the laser treatment. At the end of the treatments, all mice were kept alive until the tumors reached a maximum of tenfold the original size, or were sacrificed after the study was complete.

In Vivo Imaging: For fluorescence imaging experiments all mice were anesthetized with 4% isoflurane and maintained at 2% during imaging. Tumors were injected 4 times with 10 μL SRB:Gd-DTPA:OX PoP liposomes. Mice were then imaged with an IVIS imaging system (excitation, 535; emission, DsRed filter).

MR imaging experiments were carried out independently at a different site on a 4.7 Tesla preclinical imager using the ParaVision imaging platform (Bruker Biospin, Billerica, MA) and a custom made, 35 mm I.D. quadrature transceiver coil (m2m Imaging, Cleveland OH). T1 and T2 rates of the nanoparticles (control, + laser, + detergent) were measured at increasing concentrations at both 25 and 37 °C using an inversion-recovery, balanced steady-state free-precession scan, and a multiecho CPMG scan, respectively, as described elsewhere.[75] Relaxivities were calculated using linear regression between the measured rates versus concentration of gadolinium. For in vivo experiments, ≈1×10^6 Colon 26 (CT26.WT, ATCC) cells were injected subcutaneously into the right flank of BALB/c mice and tumor was allowed to grow until its maximum diameter reached 1–1.5 cm. Mice were anesthetized with 4% isoflurane and maintained at 2% during imaging. Body temperature was maintained by using an MR-compatible heating system (SA Instruments, Stony Brook, NY). Two NMR tubes containing CuSO4-doped 1% agarose were included for signal normalization.

Following scout scans, a baseline, T1-weighted spoiled gradient echo scan was acquired with the following parameters: echo time = 3 ms, repetition time = 15 ms, flip angle = 40°, matrix size = 192 × 128 × 128, field of view = 48 × 32 × 32 mm. After baseline imaging, 20 μl of the liposomes was injected intratumorally from the superior and inferior directions. Mice were reimaged immediately postinjection and imaging was repeated daily up to 72 h.

Histogram analysis of postinjection imaging data within the tumor suggested two populations of voxels, high intensity at the location of injection, and low intensity in regions that did not initially enhance. The two voxel populations were fit using a two-peak, Gaussian curve model in MATLAB and the tumor image data were segmented using the intermode intensity as a threshold.[76] Examination of curve fit residuals of the nonenhancing population indicated a subpopulation of voxels of slightly higher intensity than the bulk of nonenhanced tumor voxels. An additional two-peak Gaussian curve-fit model was applied to the voxels in the nonenhancing/minimally enhancing population and the data were segmented at the intersection of the Gaussian curves. This intersection correlated well with a sharp increase in residual values from the initial histogram segmentation. Identical processing was applied to the MR data acquired 24 h postinjection. Segmented image data were pseudocolorized in Analyze 7.0 (AnalyzeDirect, Figure S6, Supporting Information, middle panel) and 3D surface models generated in Amira 5.2 (FEI, Figure S6, Supporting Information, right panel).

Supporting Information

Supporting Information is available from the Wiley Online Library or from the author.

Acknowledgements

This work was supported by the National Institutes of Health (Nos. R01EB017270, DP5OD017898, and P30CA016056), the National Science Foundation (No. 1555220), and a Brazilian CAPES Science without Borders scholarship. The authors thank Dr. Thaddeus Szczesny for assistance with electron microscopy.

Conflict of Interest

The authors declare no conflict of interest.

Keywords

chemo-phototherapy, intratumoral, light-triggered, liposomes, oxaliplatin

Received: February 24, 2017
Revised: April 7, 2017
Published online: May 15, 2017

[1] W. Y. Lau, T. W. Leung, S. C. Yu, S. K. Ho, *Ann. Surg.* **2003**, *237*, 171.
[2] R. B. Thandassery, U. Goenka, M. K. Goenka, *J. Clin. Exp. Hepatol.* **2014**, *4*, S104.
[3] A. H. Mahnken, P. Bruners, R. W. Gunther, *Dig. Dis.* **2009**, *27*, 148.
[4] R. Lencioni, F. Pinto, N. Armillotta, A. M. Bassi, M. Moretti, M. Di Giulio, S. Marchi, M. Uliana, S. Della Capanna, M. Lencioni, C. Bartolozzi, *Eur. Radiol.* **1997**, *7*, 514.
[5] C. Bartolozzi, R. Lencioni, D. Caramella, C. Vignali, R. Cioni, S. Mazzeo, M. Carrai, G. Maltinti, A. Capria, P. F. Conte, *Radiology* **1995**, *197*, 812.
[6] A. Castells, J. Bruix, C. Bru, J. Fuster, R. Vilana, M. Navasa, C. Ayuso, L. Boix, J. Visa, J. Rodes, *Hepatology* **1993**, *18*, 1121.
[7] T. Livraghi, L. Bolondi, S. Lazzaroni, G. Marin, A. Morabito, G. L. Rapaccini, A. Salmi, G. Torzilli, *Cancer* **1992**, *69*, 925.
[8] H. Isobe, H. Sakai, Y. Imari, M. Ikeda, S. Shiomichi, H. Nawata, *J. Clin. Gastroenterol.* **1994**, *18*, 122.
[9] S. Shiina, K. Tagawa, Y. Niwa, T. Unuma, Y. Komatsu, K. Yoshiura, E. Hamada, M. Takahashi, Y. Shiratori, A. Terano, *AJR, Am. J. Roentgenol.* **1993**, *160*, 1023.

[10] J. S. Bhullar, G. Subhas, S. Chaudhary, B. Silberberg, J. Tilak, M. Decker, V. K. Mittal, *World J. Urol.* **2013**, *31*, 331.
[11] K. Ohnishi, N. Ohyama, S. Ito, K. Fujiwara, *Radiology* **1994**, *193*, 747.
[12] K. Ohnishi, H. Yoshioka, S. Ito, K. Fujiwara, *Hepatology* **1998**, *27*, 67.
[13] T. M. Baran, B. R. Giesselman, R. Hu, M. A. Biel, T. H. Foster, *Lasers Surg. Med.* **2010**, *42*, 728.
[14] A. Pottier, E. Borghi, L. Levy, *Anticancer Res.* **2014**, *34*, 443.
[15] J. Marill, N. M. Anesary, P. Zhang, S. Vivet, E. Borghi, L. Levy, A. Pottier, *Radiat. Oncol.* **2014**, *9*, 150.
[16] A. Pottier, E. Borghi, L. Levy, *Br. J. Radiol.* **2015**, *88*, 20150171.
[17] A. Espinosa, R. Di Corato, J. Kolosnjaj-Tabi, P. Flaud, T. Pellegrino, C. Wilhelm, *ACS Nano* **2016**, *10*, 2436.
[18] J. S. Young, C. E. Lumsden, A. L. Stalker, *J. Pathol. Bacteriol.* **1950**, *62*, 313.
[19] R. K. Jain, L. T. Baxter, *Cancer Res.* **1988**, *48*, 7022.
[20] L. T. Baxter, R. K. Jain, *Microvasc. Res.* **1989**, *37*, 77.
[21] Y. Boucher, L. T. Baxter, R. K. Jain, *Cancer Res.* **1990**, *50*, 4478.
[22] C. G. Willett, Y. Boucher, E. di Tomaso, D. G. Duda, L. L. Munn, R. T. Tong, D. C. Chung, D. V. Sahani, S. P. Kalva, S. V. Kozin, M. Mino, K. S. Cohen, D. T. Scadden, A. C. Hartford, A. J. Fischman, J. W. Clark, D. P. Ryan, A. X. Zhu, L. S. Blaszkowsky, H. X. Chen, P. C. Shellito, G. Y. Lauwers, R. K. Jain, *Nat. Med.* **2004**, *10*, 145.
[23] C. H. Heldin, K. Rubin, K. Pietras, A. Ostman, *Nat. Rev. Cancer* **2004**, *4*, 806.
[24] W. Wu, H. Chen, F. Shan, J. Zhou, X. Sun, L. Zhang, T. Gong, *Mol. Pharmaceutics* **2014**, *11*, 3378.
[25] R. K. Jain, *Adv. Drug Delivery Rev.* **1997**, *26*, 71.
[26] M. F. Milosevic, A. W. Fyles, R. Wong, M. Pintilie, M. C. Kavanagh, W. Levin, L. A. Manchul, T. J. Keane, R. P. Hill, *Cancer* **1998**, *82*, 2418.
[27] R. K. Jain, R. T. Tong, L. L. Munn, *Cancer Res.* **2007**, *67*, 2729.
[28] P. A. Netti, D. A. Berk, M. A. Swartz, A. J. Grodzinsky, R. K. Jain, *Cancer Res.* **2000**, *60*, 2497.
[29] E. B. Brown, Y. Boucher, S. Nasser, R. K. Jain, *Microvasc. Res.* **2004**, *67*, 231.
[30] H. Holback, Y. Yeo, *Pharm. Res.* **2011**, *28*, 1819.
[31] T. Kitai, T. Inomoto, M. Miwa, T. Shikayama, *Breast Cancer* **2005**, *12*, 211.
[32] K. J. Harrington, G. Rowlinson-Busza, K. N. Syrigos, P. S. Uster, R. G. Vile, J. S. Stewart, *Clin. Cancer Res.* **2000**, *6*, 2528.
[33] K. A. Carter, S. Shao, M. I. Hoopes, D. Luo, B. Ahsan, V. M. Grigoryants, W. Song, H. Huang, G. Zhang, R. K. Pandey, J. Geng, B. A. Pfeifer, C. P. Scholes, J. Ortega, M. Karttunen, J. F. Lovell, *Nat. Commun.* **2014**, *5*, 3546.
[34] D. Luo, N. Li, K. A. Carter, C. Lin, J. Geng, S. Shao, W.-C. Huang, Y. Qin, G. E. Atilla-Gokcumen, J. F. Lovell, *Small* **2016**, *12*, 3039.
[35] D. Luo, K. A. Carter, A. Razi, J. Geng, S. Shao, D. Giraldo, U. Sunar, J. Ortega, J. F. Lovell, *Biomaterials* **2016**, *75*, 193.
[36] K. A. Carter, S. Wang, J. Geng, D. Luo, S. Shao, J. F. Lovell, *Mol. Pharmaceutics* **2016**, *13*, 420.
[37] S. Shao, J. Geng, H. Ah Yi, S. Gogia, S. Neelamegham, A. Jacobs, J. F. Lovell, *Nat. Chem.* **2015**, *7*, 438.
[38] J. Rieffel, F. Chen, J. Kim, G. Chen, W. Shao, S. Shao, U. Chitgupi, R. Hernandez, S. A. Graves, R. J. Nickles, P. N. Prasad, C. Kim, W. Cai, J. F. Lovell, *Adv. Mater.* **2015**, *27*, 1785.
[39] K. A. Carter, D. Luo, A. Razi, J. Geng, S. Shao, J. Ortega, J. F. Lovell, *Theranostics* **2016**, *6*, 2329.
[40] D. Luo, K. A. Carter, A. Razi, J. Geng, S. Shao, C. Lin, J. Ortega, J. F. Lovell, *J. Controlled Release* **2015**, *220*, 484.
[41] S. Shao, T. N. Do, A. Razi, U. Chitgupi, J. Geng, R. J. Alsop, B. G. Dzikovski, M. C. Rheinstädter, J. Ortega, M. Karttunen, J. A. Spernyak, J. F. Lovell, *Small* **2017**, *13*, 1602505.
[42] D. Luo, K. A. Carter, D. Miranda, J. F. Lovell, *Adv. Sci.* **2017**, *4*, 1600106.
[43] B. P. Timko, T. Dvir, D. S. Kohane, *Adv. Mater.* **2010**, *22*, 4925.
[44] A. Y. Rwei, W. Wang, D. S. Kohane, *Nano Today* **2015**, *10*, 451.
[45] J. You, G. Zhang, C. Li, *ACS Nano* **2010**, *4*, 1033.
[46] N. Fomina, J. Sankaranarayanan, A. Almutairi, *Adv. Drug Delivery Rev.* **2012**, *64*, 1005.
[47] B. Q. Spring, R. Bryan Sears, L. Z. Zheng, Z. Mai, R. Watanabe, M. E. Sherwood, D. A. Schoenfeld, B. W. Pogue, S. P. Pereira, E. Villa, T. Hasan, *Nat. Nanotechnol.* **2016**, *11*, 378.
[48] K. Lu, C. He, N. Guo, C. Chan, K. Ni, R. R. Weichselbaum, W. Lin, *J. Am. Chem. Soc.* **2016**, *138*, 12502.
[49] S. Fang, J. Lin, C. Li, P. Huang, W. Hou, C. Zhang, J. Liu, S. Huang, Y. Luo, W. Fan, D. Cui, Y. Xu, Z. Li, *Small* **2017**, *13*, 1602580.
[50] F. Mao, L. Wen, C. Sun, S. Zhang, G. Wang, J. Zeng, Y. Wang, J. Ma, M. Gao, Z. Li, *ACS Nano* **2016**, *10*, 11145.
[51] G. Bao, S. Mitragotri, S. Tong, *Annu. Rev. Biomed. Eng.* **2013**, *15*, 253.
[52] H. Xing, W. Bu, S. Zhang, X. Zheng, M. Li, F. Chen, Q. He, L. Zhou, W. Peng, Y. Hua, J. Shi, *Biomaterials* **2012**, *33*, 1079.
[53] Y. Lyu, Y. Fang, Q. Miao, X. Zhen, D. Ding, K. Pu, *ACS Nano* **2016**, *10*, 4472.
[54] P. Huang, J. Lin, X. Wang, Z. Wang, C. Zhang, M. He, K. Wang, F. Chen, Z. Li, G. Shen, D. Cui, X. Chen, *Adv. Mater.* **2012**, *24*, 5104.
[55] R. Mo, T. Jiang, R. DiSanto, W. Tai, Z. Gu, *Nat. Commun.* **2014**, *5*, 3364.
[56] C. Qian, J. Yu, Y. Chen, Q. Hu, X. Xiao, W. Sun, C. Wang, P. Feng, Q.-D. Shen, Z. Gu, *Adv. Mater.* **2016**, *28*, 3313.
[57] J. Liu, W. Bu, L. Pan, J. Shi, *Angew. Chem., Int. Ed.* **2013**, *52*, 4375.
[58] S. Wang, P. Huang, X. Chen, *ACS Nano* **2016**, *10*, 2991.
[59] W. Tao, X. Zhu, X. Yu, X. Zeng, Q. Xiao, X. Zhang, X. Ji, X. Wang, J. Shi, H. Zhang, L. Mei, *Adv. Mater.* **2017**, *29*, 1603276.
[60] J. Rieffel, U. Chitgupi, J. F. Lovell, *Small* **2015**, *11*, 4445.
[61] T. Lajunen, L. S. Kontturi, L. Viitala, M. Manna, O. Cramariuc, T. Rog, A. Bunker, T. Laaksonen, T. Viitala, L. Murtomaki, A. Urtti, *Mol. Pharmaceutics* **2016**, *13*, 2095.
[62] D. Miranda, J. F. Lovell, *Bioeng. Transl. Med.* **2016**, *1*, 267.
[63] J. Chen, H. Jiang, Y. Wu, Y. Li, Y. Gao, *Drug Des., Dev. Ther.* **2015**, *9*, 2265.
[64] S. Zalba, I. Navarro, I. F. Trocóniz, C. Tros de Ilarduya, M. J. Garrido, *Eur. J. Pharm. Biopharm.* **2012**, *81*, 273.
[65] K. Un, K. Sakai-Kato, Y. Oshima, T. Kawanishi, H. Okuda, *Biomaterials* **2012**, *33*, 8131.
[66] T. D. Yang, W. Choi, T. H. Yoon, K. J. Lee, J. S. Lee, J. H. Joo, M. G. Lee, H. S. Yim, K. M. Choi, B. Kim, J. J. Lee, H. Kim, D. Y. Lee, K. Y. Jung, S. K. Baek, *Biomed. Opt. Express* **2016**, *7*, 185.
[67] A. S. Abu Lila, S. Kizuki, Y. Doi, T. Suzuki, T. Ishida, H. Kiwada, *J. Controlled Release* **2009**, *137*, 8.
[68] J. F. Lovell, C. S. Jin, E. Huynh, H. Jin, C. Kim, J. L. Rubinstein, W. C. W. Chan, W. Cao, L. V. Wang, G. Zheng, *Nat. Mater.* **2011**, *10*, 324.
[69] J. R. Reichenbach, T. Hacklander, T. Harth, M. Hofer, M. Rassek, U. Modder, *Eur. Radiol.* **1997**, *7*, 264.
[70] P. Caravan, J. J. Ellison, T. J. McMurry, R. B. Lauffer, *Chem. Rev.* **1999**, *99*, 2293.
[71] V. Jacques, S. Dumas, W. C. Sun, J. S. Troughton, M. T. Greenfield, P. Caravan, *Invest. Radiol.* **2010**, *45*, 613.
[72] M. Hossann, T. Wang, Z. Syunyaeva, M. Wiggenhorn, A. Zengerle, R. D. Issels, M. Reiser, L. H. Lindner, M. Peller, *J. Controlled Release* **2013**, *166*, 22.
[73] A. E. Yassin, M. K. Anwer, H. A. Mowafy, I. M. El-Bagory, M. A. Bayomi, I. A. Alsarra, *Int. J. Med. Sci.* **2010**, *7*, 398.
[74] E. G. Bligh, W. J. Dyer, *Can. J. Biochem. Physiol.* **1959**, *37*, 911.
[75] S. J. Dorazio, P. B. Tsitovich, K. E. Siters, J. A. Spernyak, J. R. Morrow, *J. Am. Chem. Soc.* **2011**, *133*, 14154.
[76] J. M. Prewitt, M. L. Mendelsohn, *Ann. N. Y. Acad. Sci.* **1966**, *128*, 1035.

